Phase modulation in pulsed dual-frequency capacitively coupled plasmas

De-Qi Wen,[1] Quan-Zhi Zhang,[1] Wei Jiang,[2] Yuan-Hong Song,[1] Annemie Bogaerts,[3] and You-Nian Wang[1,a)]

[1]*School of Physics and Optoelectronic Technology, Dalian University of Technology, Dalian 116024, People's Republic of China*

[2]*School of Physics, Huazhong University of Science and Technology, Wuhan 430074, People's Republic of China*

[3]*Research group PLASMANT, Department of Chemistry, University of Antwerp, Universiteitsplein 1, BE-2610Wilrijk-Antwerp, Belgium*

(Received 28 March 2014; accepted 7 June 2014; published online 19 June 2014)

Particle-in-cell/Monte Carlo collision simulations, coupled with an external circuit, are used to investigate the behavior of pulsed dual-frequency (DF) capacitively coupled plasmas (CCPs). It is found that the phase shift θ between the high (or low) frequency source and the pulse modulation has a great influence on the ion density and the ionization rate. By pulsing the high frequency source, the time-averaged ion density shows a maximum when $\theta = 90^\circ$. The time-averaged ion energy distribution functions (IEDFs) at the driven electrode, however, keep almost unchanged, illustrating the potential of pulsed DF-CCP for independent control of ion density (and flux) and ion energy. A detailed investigation of the temporal evolution of the plasma characteristics indicates that several high frequency harmonics can be excited at the initial stage of a pulse period by tuning the phase shift θ, and this gives rise to strong sheath oscillations, and therefore high ionization rates. For comparison, the pulsing of the low frequency source is also studied. In this case, the ion density changes slightly as a function of time, and the time-averaged ion density shows the same trend as in the HF modulation for different phase shifts θ. Moreover, the time-averaged IEDFs at the driven electrode can be modulated, showing the potential to reduce the maximum ion bombardment energy. © *2014 AIP Publishing LLC*. [http://dx.doi.org/10.1063/1.4884225]

I. INTRODUCTION

Capacitively coupled radio-frequency (CCRF) discharges are commonly used for plasma etching in microelectronics technology.[1] Of importance to the etching processes is the ion flux and energy bombing the electrodes. A high ion flux, determined by high plasma densities, is desired for high manufacturing throughput, while the ion bombardment energy needs to be controlled independently to avoid damaging the material.[1] Improvements in controlling these key plasma parameters are essential because of the decreasing line width and the increasing size of the wafers,[2] and a lot of researchers have been working on this topic.[3–32] Dual-frequency capacitively coupled plasmas (DF CCPs), i.e., driving the plasma with two substantially different radio frequencies, from which the low frequency component controls the ion energy and the high frequency determines the plasma density, are introduced as a promising way to achieve this separate control.[3–7] However, the coupling of both frequencies[8–15] and the effect of secondary electrons[7,15,16] place a limitation to realizing this goal. Czarnetzki *et al.*[16–21] proposed a flexible method to control the ion properties by the so-called electrical asymmetry effect (EAE) in geometrically symmetric discharges and demonstrated that the dc self-bias could be controlled by driving one electrode with the fundamental frequency and its even harmonic. Similarly to the idea of the EAE, which changes the voltage waveform on the powered electrode, pulsed modulation in CCRF discharges has shown its potential in improving the etch profile characteristics with high aspect ratio, as it can provide high flexibility by adjusting the frequency and the duty cycle,[22] and therefore it has attracted increasing academic and industrial interest in recent years.[1,23–32]

Numerical investigations on pulsed plasma sources can help us to improve our fundamental understanding of discharge mechanisms and to find suitable modulation parameters for better etch processes. It has been shown in a global model that, in argon plasmas driven by time modulated power, higher time-averaged plasma densities can be obtained than those in continuous wave (CW) plasmas.[23] Agarwal *et al.*[24] demonstrated by means of a two-dimensional fluid model of a pulsed dual-frequency (DF) CCP that the Ar/CF_4 plasma uniformity can be controlled, to a certain degree, by modulating the phase lag between the pulsed high and low frequency powers. Further simulations from the same group focused on the influence of pulse frequency and gas composition on the negative ion flux to the wafer and suggested that a long afterglow period is necessary for negative ion extraction into the wafer features.[25] Kim *et al.*[26] predicted by particle-in-cell/ Monte Carlo (PIC/MCC) simulations for a CCP that the pulsed rf form of the driving current could induce a discharge asymmetry, i.e., the time-averaged plasma density peaks off the center between the two electrodes and a self-bias develops at the powered electrode. Recently, Lafleur *et al.*[27,28] computationally demonstrated that the power deposition, the plasma density and ion fluxes can be increased by using Gaussian-shaped voltage pulses instead of sinusoidal waveforms. Furthermore, an

a)E-mail: ynwang@dlut.edu.cn

asymmetry in the ion fluxes to the powered and grounded electrodes was created at increasing pressure. The average ion bombardment energy, however, remained almost constant. Finally, based on PIC/MCC simulations, control of the ion energy distribution (IED) on the substrate electrode can be achieved in the afterglow of a pulsed CCP, which will be beneficial to plasma processing.[29] In addition, the periodic interruption of the driving frequency leads to temporal changes in the plasma parameters.

The initial stage of a pulse period is critical for the process, because in this stage the plasma parameters change dramatically, for example, a bias voltage is formed on the blocking capacitor,[30] and the electron temperature rapidly increases above the steady state value.[31,32] Therefore, a more systematic investigation, especially at the initial stage of a pulsed discharge, is needed to understand the discharge dynamics and temporal evolution of plasma parameters. This can not only provide a better physical insight, but it can also give information about the optimum operating conditions. However, in spite of the fact that pulsed plasmas are widely investigated, most of these studies are focused on pulsed single frequency (SF) CCPs,[26–30,32] while only a few of them correspond to pulsed dual frequency CCPs.[24,25,31] Especially, the way in which the phase shift between the two frequency sources and the pulse affects the plasma behavior is still not fully understood.

In this work, the discharge properties of a pulsed DF (60 MHz/2 MHz) CCP are investigated by means of self-consistent PIC/MCC simulations. We will study in detail the effects of phase modulation between high (or low) frequency source and the pulse on plasma parameters. The relationship between the plasma density, ion energy, discharge asymmetry, and phase shift of the pulse modulation will also be investigated. Our paper is organized as follows: the simulation details and discharge parameters are outlined in Sec. II. In Sec. III, the simulation results are presented, and a short conclusion is drawn in Sec. IV.

II. DESCRIPTION OF THE PIC/MCC SIMULATIONS

Simulations were performed by using a standard 1d3v (i.e., one-dimensional in space and three-dimensional in velocity) electrostatic PIC method, coupled with a MCC model and an external circuit.[33,34] The external circuit contains a bias capacitor (C_B with a value of 2 nF). The model is a self-consistent and fully kinetic model, which forms part of the "multi-physics analysis of plasma sources" (MAPS) code developed by Wang and coworkers.[35–38] Our simulations are applied to an argon discharge with a gap between the two electrodes of 4 cm. The rf/pulse voltage source is connected with the electrode at the position of $z = 0$ cm through a bias capacitor (C_B), and the grounded electrode is at $z = 4$ cm, as shown in Figure 1. The potential at the powered electrode is self-consistently obtained.[33] According to Kirchhoff's voltage law:

$$V_C(t) = V(t) - \phi_0(t), \tag{1}$$

where $V_C(t)$ is the voltage drop across the capacitor C_B, $V(t)$ is the applied voltage source, and $\phi_0(t)$ is the potential at the powered electrode ($z = 0$). The electric current at the powered electrode satisfies the continuity equation given by Eq. (2). Q is the charge at the powered electrode ($z = 0$), $I(t)$ and $I_{conv}(t)$ are the external circuit current and the convective current arriving at the powered electrode, respectively. Gauss' law near the electrode can be written as Eq. (3), and **E** is the electric field

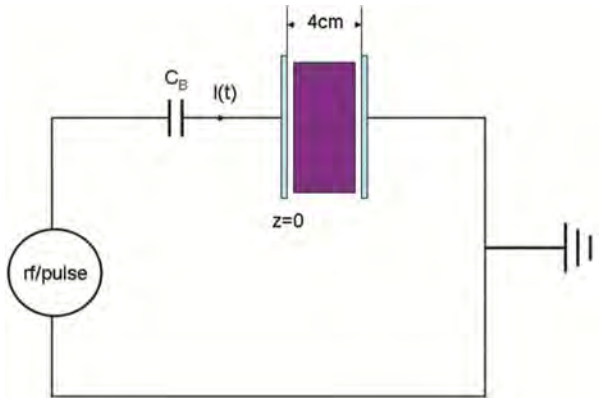

FIG. 1. Schematic picture of the CCP and external circuit, showing the rf and the pulsed rf voltage source (rf/pulse), and the bias capacitor (C_B). $I(t)$ is the current flowing in the external circuit.

$$\frac{dQ}{dt} = I(t) + I_{conv}(t), \tag{2}$$

$$\epsilon_0 \oint_S \mathbf{E} \cdot \mathbf{dS} = \mathbf{Q}. \tag{3}$$

Finally, Poisson's equation in the plasma is as follows:

$$\epsilon_0 \nabla^2 P(x,t) = \tilde{\rho}(x,t), \tag{4}$$

$$\epsilon_0 \nabla^2 L(x,t) = 0. \tag{5}$$

$P(z=0)=0$, $P(z=4)=0$ and $L(z=0)=1$, $L(z=4)=0$ are the boundary conditions of Eqs. (4) and (5), respectively. $P(x,t)$ is the potential generated by the charge in plasma and $L(x,t)$ is the vacuum potential determined by the applied boundary conditions. Thus, the powered electrode potential $\phi_0(t)$ is obtained by solving Eqs. (1)–(5) and the plasma potential $\phi(t)$ is calculated by

$$\phi(x,t) = P(x,t) + \phi_0(t)L(x,t). \tag{6}$$

When the high frequency (HF) source is modulated, the voltage waveform (i.e., $V(t)$) is given by

$$V_H(t) = g(t,\theta)V_{HF}(t) + V_{LF}(t). \tag{7}$$

Similarly, when the low frequency (LF) source is modulated, the voltage waveform is expressed by

$$V_L(t) = g(t,\theta)V_{LF}(t) + V_{HF}(t). \tag{8}$$

In both equations, $V_{HF}(t) = V_{H0}\sin(2\pi f_{HF}t)$ and $V_{LF}(t) = V_{L0}\sin(2\pi f_{LF}t)$, $g(t,\theta)$ is the pulse modulation factor (i.e., the on-off switch of the HF or LF source) given by Eq. (9); they are all plotted as a function of time in Figure 2(a).

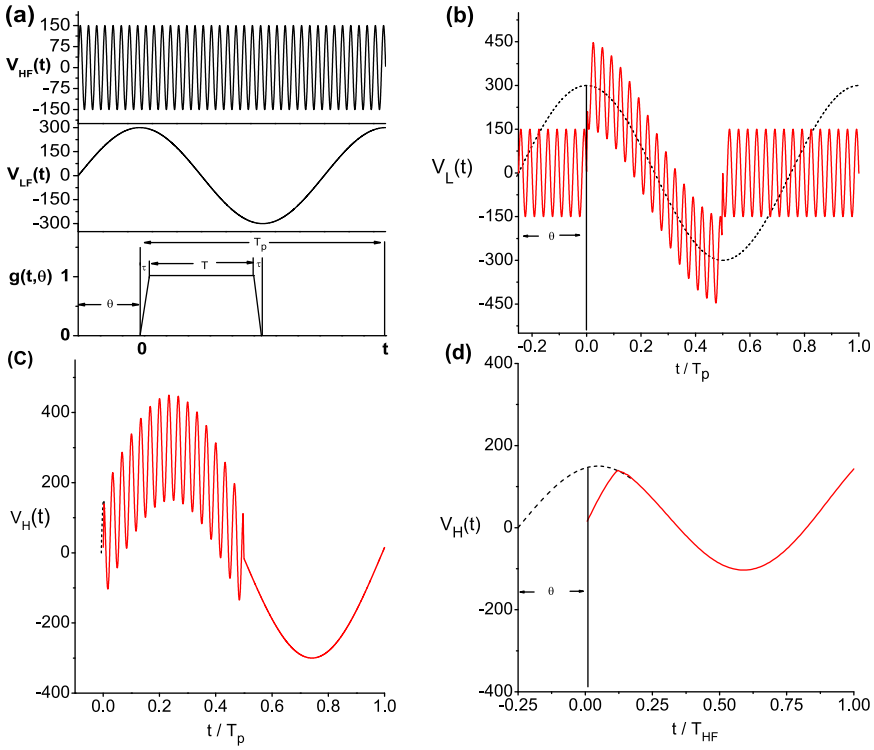

FIG. 2. (a) Schematic diagram of the modulated voltage waveform (see text for more explanation). (b) and (c) Illustration of LF and HF pulse modulation, respectively, for the pulse modulation factor of (a). (d) is a zoomed part of (c) in the first HF period.

$$g(t,\theta) = \begin{cases} t/\tau & (0 \le t < \tau), \\ 1 & (\tau \le t < T+\tau), \\ 1-(t-T-\tau)/\tau & (T+\tau \le t < T+2\tau), \\ 0 & (T+2\tau \le t < T_p). \end{cases} \quad (9)$$

Note that 0 indicates the start of the pulse modulation, τ stands for the rise and fall times, which are taken equal in our case, T is the plateau value of the pulse modulation factor, and T_p is the total pulse modulation period, consisting of pulse-on and pulse-off time. θ is the phase shift between the HF source and the start of the pulse modulation for HF modulation, or in the case of LF modulation, it is the phase shift between the LF source and the start of the pulse for LF modulation. This phase difference varies from 0° to 180°. The rise (and fall) time τ is fixed to $0.1T_{HF}$, where $T_{HF} = f_{HF}^{-1}$. In addition, f_{HF} and f_{LF} correspond to the HF of 60 MHz and LF of 2 MHz, respectively, and V_{H0}, V_{L0}, are their voltage amplitudes. In the simulation, V_{H0} is kept at 150 V and V_{L0} is set at 300 V. In addition, the duty cycle of the pulse modulation $\eta = (T+2\tau)/T_p = 0.5$. Furthermore, the pulse repetition frequency, represented by f, varies from 200 kHz to 2 MHz.

To make this pulse modulation more clear, an illustration of the pulse modulation of the HF source ($V_H(t)$), in one LF cycle, is given in Figures 2(c) and 2(d), for the pulse modulation factor shown in Figure 2(a), whereas the pulse modulation of the LF source ($V_L(t)$), again in one LF cycle, is illustrated in Figure 2(b). The discharge is sustained at 20 mTorr. Elastic, excitation, and ionization collisions for electrons and charge transfer collisions for Ar^+ ions are taken into account in Monte Carlo part.[38–40] Multistep ionization and metastable atoms are not included in our PIC/MCC model for two reasons. First, including metastable atoms in a PIC/MCC code is computationally very time consuming.[41] Moreover, Turner *et al.*[41,42] have proven that metastable atoms do not affect the plasma density in low pressure discharges with a PIC/MCC method, and Ashida *et al.*[23] came to the same conclusion by means of a global model. We also investigated the effect of metastable atoms on plasma density with a global model under our typical simulation parameters and found that the relative error between including and excluding metastable atoms is less than one percent.

In our PIC/MCC simulation, the electron and the ion cross sections are taken from Refs. 43 and 44, respectively. The secondary-electron emission coefficient for argon ions is set to 0.12, while electrons are assumed to be perfectly absorbed at the electrodes (hence the electron-induced secondary electron emission coefficient is assumed to be zero). The initial velocities of the secondary electrons from the surfaces are calculated from the Maxwellian distribution at an average electron temperature of 3 eV. The secondary electrons are emitted toward the plasma in an isotropic way.

An explicit scheme is used in all simulations. The space step $\triangle x$ and time step $\triangle t$ are fixed to 4.0×10^{-5} m and 0.8×10^{-11} s, respectively, for $\theta = 0°$, 45°, 90°. However, for the later calculations performed with other θ values, we increased $\triangle x$ and $\triangle t$ to 8.0×10^{-5} m and 2.0×10^{-11} s, for the purpose of saving computing time. When the discharge reaches equilibrium, at least 150 super-particles in per cell are adopted, which satisfies the convergence conditions as discussed by Turner.[45] The initial electron and ion temperatures are set as 3 eV and 0.026 eV, respectively. Typically, the code is run for over 500 pulse cycles to reach equilibrium. After the system reaches equilibrium, the plasma parameters, such as the species densities, the ionization rate distributions and the currents, are calculated by statistical average of 30 pulse periods.

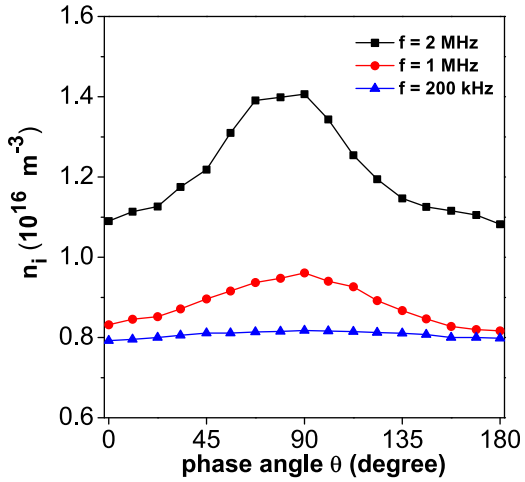

FIG. 3. Ion density versus the phase shift between the HF source and the pulse modulation for a pulse modulation frequency of 200 kHz, 1 MHz, and 2 MHz.

III. RESULTS AND DISCUSSIONS

A. High frequency modulation: Control of ion density and ion energy

The time-averaged peak values of Ar^+ density n_i at the center between the two electrodes are plotted in Figure 3 as a function of the phase shift θ between HF source and the pulse modulation, for three different pulse frequencies of 200 kHz, 1 MHz, and 2 MHz. As can be seen, the overall density n_i reaches a maxima value at $\theta = 90^\circ$, at a pulse frequency of 1 MHz and 2 MHz, but it remains almost constant at 200 kHz. Furthermore, the variation as a function of phase shift θ is higher at higher pulse frequency. This can be understood because different phase shifts θ induce different initial stages of the pulse modulation period, as will be explained in Sec. III B. Indeed, the ionization rate in the initial stage of the pulse is very low at $\theta = 0^\circ$ compared to the value $\theta = 90^\circ$. In addition, for the case of low pulse modulation frequency, there is a longer "off time," within which the heating caused by the HF sheath oscillation disappears and more charged particles become lost at electrodes due to the absence of the HF sheath. This explains why a lower pulse modulation frequency gives rise to a lower average ion density at a fixed shift θ.

Figure 4(a) shows the time-averaged ion energy distribution functions (IEDFs) at the driven electrode, for a pulse repetition frequency of $f = 2$ MHz and three different values of the phase shift θ between the HF source and the pulse modulation. It can be seen that the IEDFs are almost identical at different values of θ. This is because the temporal evolution of the sheath potential has approximately the same shape (as shown in Figure 4(b)). Note that the sheath potential is defined by the difference between the driven electrode potential and the maximum potential in the plasma.

It is indeed clear that the two peaks in Figure 4(a) indicated with "1" and "2," are determined by $-|V_{min}|$ and $-|V_{max}|$ in Figure 4(b), respectively. Since $-|V_{min}|$ and $-|V_{max}|$ are practically the same for the different phase shifts, it is logical that the IEDFs are also almost identical. The many peaks in Figure 4(a) are caused by charge-exchange collisions between ions and neutral atoms.[46,47]

Thus, it is clear that by pulsing the HF source in DF CCPs, the ion density can be adjusted by varying the pulse modulation repetition frequency and the phase shift between the HF source and the pulse modulation, while the IEDFs approximately stay constant.

B. High frequency modulation: Temporal evolution of the plasma characteristics

The temporal evolution of the spatially averaged densities of Ar^+ ions within one pulse modulation period is shown in Figure 5(a) for different values of the phase shift between the HF source and the pulse modulation factor, i.e., $\theta = 0^\circ$, 22.5°, 45°, 67.5°, 90°. Note that the pulse-on time is for $t < 0.5T_p$. For $\theta = 0^\circ$, the spatially averaged density increases almost linearly with time as soon as the pulse is switched on, and subsequently it decreases as the pulse is switched off. When θ rises from 0° to 90°, the ion densities distinctly increase with time in the early parts of the pulse modulation, after which the rise becomes more gradual until the end of the pulse. The temporal behavior of the ion densities can be explained by the corresponding temporal ionization rates over the pulse period, which is shown in Figure 5(b). Indeed, the

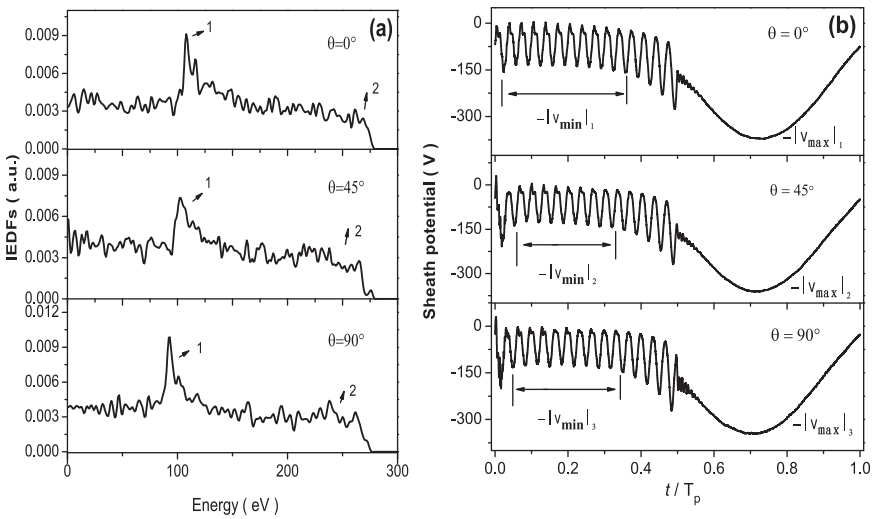

FIG. 4. (a) Time-averaged ion energy distribution functions (IEDFs) at the driven electrode, and (b) temporal sheath potential in one pulse period, for a pulse repetition frequency of $f = 2$ MHz, and three different values of the phase shift between the HF source and the pulse modulation, i.e., $\theta = 0^\circ$, 45°, 90°.

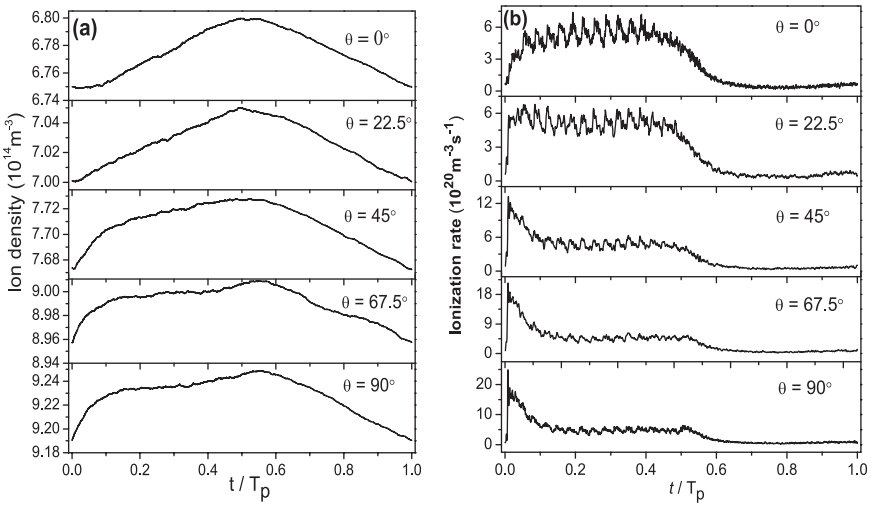

FIG. 5. Spatially averaged (a) Ar^+ densities and (b) ionization rates at 20 mTorr as a function of time within one pulse modulation period for different phase shifts between the HF source and the pulse modulation factor, using a pulse modulation frequency of 2 MHz, and 50% duty cycle.

ionization rate increases slowly at the beginning of the pulse and gradually reaches steady state for a phase shift $\theta = 0°$, while it rises extremely rapidly to a value of three times the steady state value, for a phase shift $\theta = 90°$. This indicates that a lot of high-energy electrons have been generated in the initial stage of the pulse modulation at $\theta = 90°$. We will further explain this later in the paper.

In addition, we can see that the ion density does not decrease instantly when the pulse is switched off ($t = 0.5T_p$), but the drop starts only at about $t = 0.55T_p$ in Figure 5(a). This can be explained by two reasons: on one hand, the "fall time" of the pulse causes a delay in the drop of the ionization so that still ions are created, and on the other hand, the electrons cool down extremely rapidly after the pulse is switched off,[23,31,32,48] which considerably reduces their diffusion. Hence, the electrons (as well as the ions) stay a bit longer in the plasma, explaining why the drop is somewhat delayed.

In order to better understand the underlying physics of the enhanced ionization in the initial stage of pulse period, we analyze the spatiotemporal ionization rates and the temporal currents. The spatiotemporal ionization rates of the first HF period and the second last HF period during the pulse-on time are shown in Figure 6 for $\theta = 0°$ (a1, a2, respectively) and $\theta = 90°$ (b1, b2, respectively). As can be seen from Figures 6(a1) and 6(b1), the maximum ionization mainly occurs close to the driven electrode ($z = 0$ cm), i.e., the discharge is asymmetric within the first HF period. As time evolves, the discharge gradually becomes more symmetric, as is shown in Figures 6(a2) and 6(b2) for the second last HF period. The comparison of Figures 6(a1), 6(b1) with Figures 6(a2), 6(b2) makes it clear that the ionization rate in the beginning of the pulse modulation is larger than at the end of the pulse modulation, especially at $\theta = 90°$, where the maximum ionization rate is 10 times larger in Figures 6(b1) than 6(b2). Moreover, two electron beams close to each other

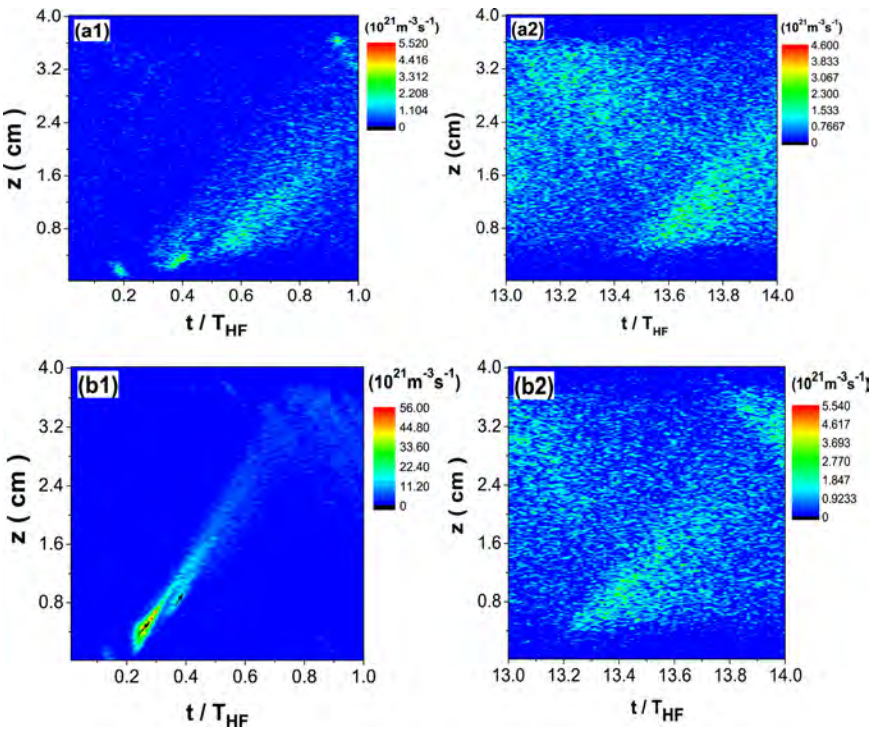

FIG. 6. Spatiotemporal ionization rates: (a1) 1 HF period (T_{HF}) in the beginning and (a2) 1 HF period at the end of the pulse-on time, both for a phase shift $\theta = 0°$, (b1) and (b2) correspond to the case of $\theta = 90°$.

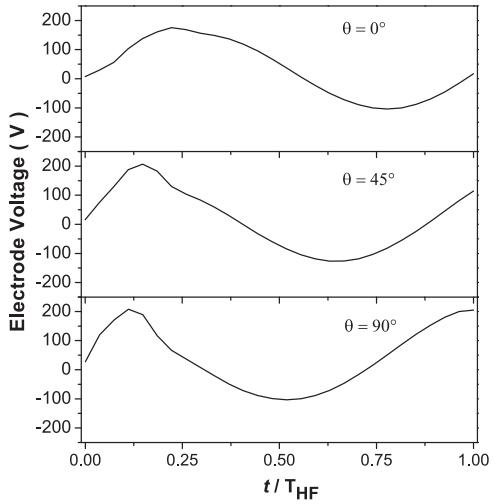

FIG. 7. Driven electrode potential in the first HF period of the pulse modulation, at three different phase shifts between HF source and pulse modulation.

(indicated with two black arrows) can be clearly seen in Figure 6(b1), which give rise to very high ionization rate near $t = 0.2T_{HF}$ and $t = 0.4T_{HF}$.

In DF CCPs driven by continuous waves, the main heating mechanism is collisionless (or stochastic), which can produce high-energy electrons at the oscillating plasma sheath boundaries, at typical pressures around 20 mTorr.[10,49,50]

In the case of pulsed DF CCPs, the high ionization rate can be explained because several HF harmonics can be excited (see below), which induce several rapid expansions of the sheath. These expansions of the sheath are much faster than the sheath expansion caused by just the fundamental driving rf frequency. In this way, fast beam electrons, which travel from the sheath region toward the plasma bulk, are created and the ionization is strongly enhanced.

The reason for the excitation of the HF harmonics can be explained as follows: in typical CCPs, there is a

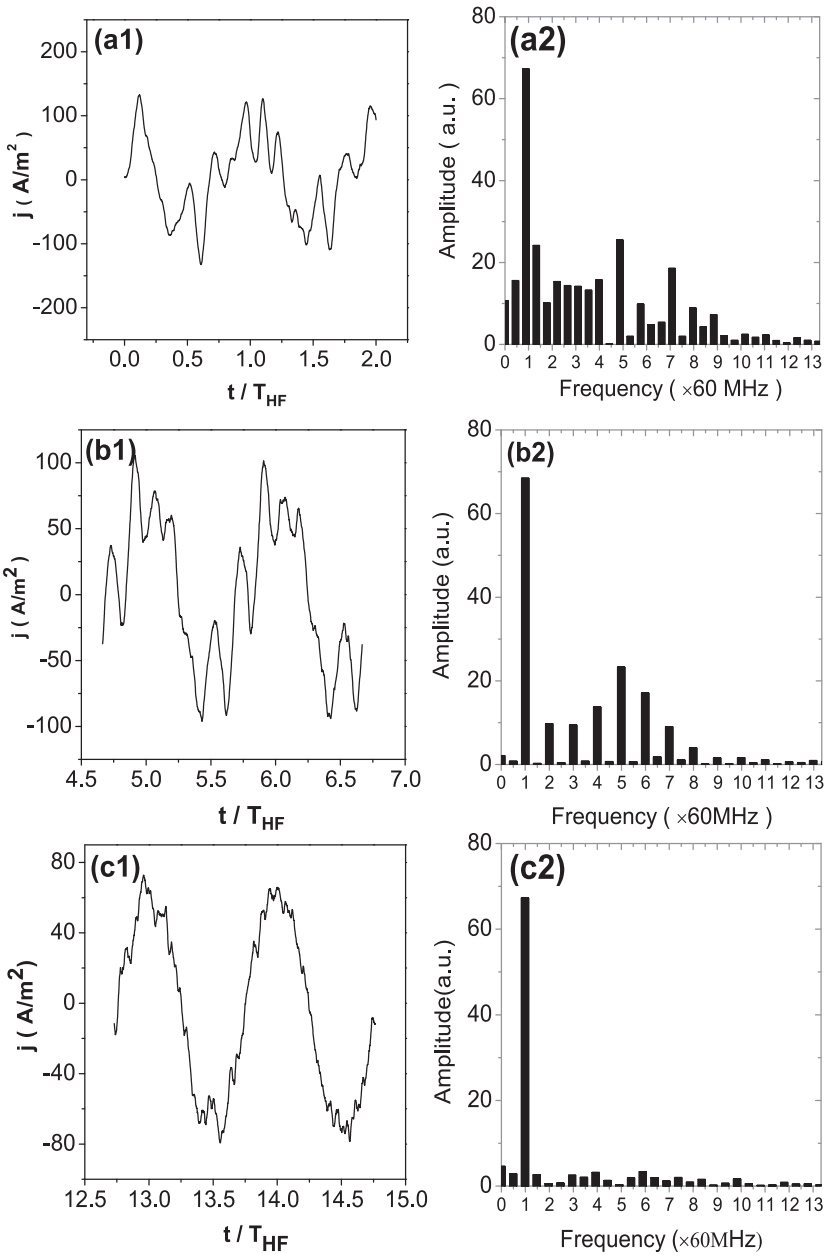

FIG. 8. (a1), (b1), (c1): Two full cycles of the HF current picked up at the centre of the two electrodes with $\theta = 0°$. (a2), (b2), (c2): Fourier components of the current correspond to (a1), (b1), (c1), respectively. The components corresponding to the applied HF voltage at 60 MHz shows clearly visible from beginning to the end. (a1) shows the first two HF periods, (b1) shows the middle two ones with the pulse-on; (c1) shows the two ones at the end of pulse-on.

nonlinear charge-voltage relation in an individual sheath.[1,18,20] Generally, the nonlinearity cancels for the sum of both sheath voltages in symmetric discharges.[1] However, in our case, the pulse has a fixed rising/falling time between pulse-on and pulse-off, which means that when modulating the rf voltage, the voltage value will change from 0 to the normal rf voltage value rapidly within a small rise/fall time. This makes the voltage waveform in the first HF period asymmetric[18,20] for different phase shifts θ, as shown in Figure 7. This lead to a strong asymmetry between the sheaths, and the HF harmonics are thus excited. Besides, we can see from Figure 7 that the asymmetry of the voltage waveform in the first HF period is weak at $\theta = 0^\circ$, but very strong at $\theta = 90^\circ$, which explains the much larger ionization rate at $\theta = 90^\circ$ than at $\theta = 0^\circ$, as shown in Figures 6(b1) and 6(a1).

To further elucidate the generation of the HF harmonics, we show the temporal current at the center point between two electrodes at $\theta = 0^\circ$ in Figures 8(a1), 8(b1), and 8(c1), corresponding to the first two HF periods, two HF periods at the middle stages, and the last two HF periods within the pulse-on time. The total pulse-on time contains 15 HF periods. Figures 8(a2), 8(b2), and 8(c2) display the corresponding absolute values of the Fourier components of the currents shown in Figures 8(a1), 8(b1), and 8(c1), respectively.

As can be seen in Figure 8(a1), besides the normal HF component (i.e., 60 MHz), there are also higher frequency components, i.e., five times and eight times the basic frequency, as can be deduced from Figure 8(a2).

From the evolution of Fourier components over time during the pulse-on period, shown in Figures 8(a2), 8(b2), and 8(c2), we conclude that many HF harmonics are generated in the first two HF period, but they gradually fade away, leaving only the harmonics with an integer times the basic frequency, as shown in Figure 8(b2). Finally, in the last two HF periods (Figure 8(c2)) of pulse-on time, the HF harmonics have nearly disappeared and only the 60 MHz frequency component remains. The 2 MHz component is too small to be seen.

The HF current at the center between both electrodes, as a function of time during the first three HF periods, as well as the Fourier components, in the case of $\theta = 90^\circ$ is illustrated in Figures 9(a1) and 9(a2). Obviously, more and stronger frequency components relative to the case at $\theta = 0^\circ$ are visible. This is because the voltage difference for the change in the rise time of the pulse is much larger at $\theta = 90^\circ$ than at $\theta = 0^\circ$, and the larger voltage difference induces a stronger asymmetry between the two sheaths. This is also the reason for the much higher ionization rate at $\theta = 90^\circ$ than at $\theta = 0^\circ$, as shown in Figures 6(a1) and 6(b1).

To examine the effect of rise time in detail, we have also performed calculations with a rise time reduced to 0 at $\theta = 90^\circ$, which means that the HF voltage rises instantaneously from 0 to its normal value. The calculated HF current as a function of time during the first three HF periods, as well as its Fourier components, are plotted in Figures 9(b1) and 9(b2). It is evident that even higher frequency components are now excited compared to the case with a small rise time. Hence, a shorter rise time induces more and stronger HF harmonics and consequently this would extremely enhance the ionization. We have seen that this phenomenon is widespread, even though the repetition frequency drops to 200 kHz, since

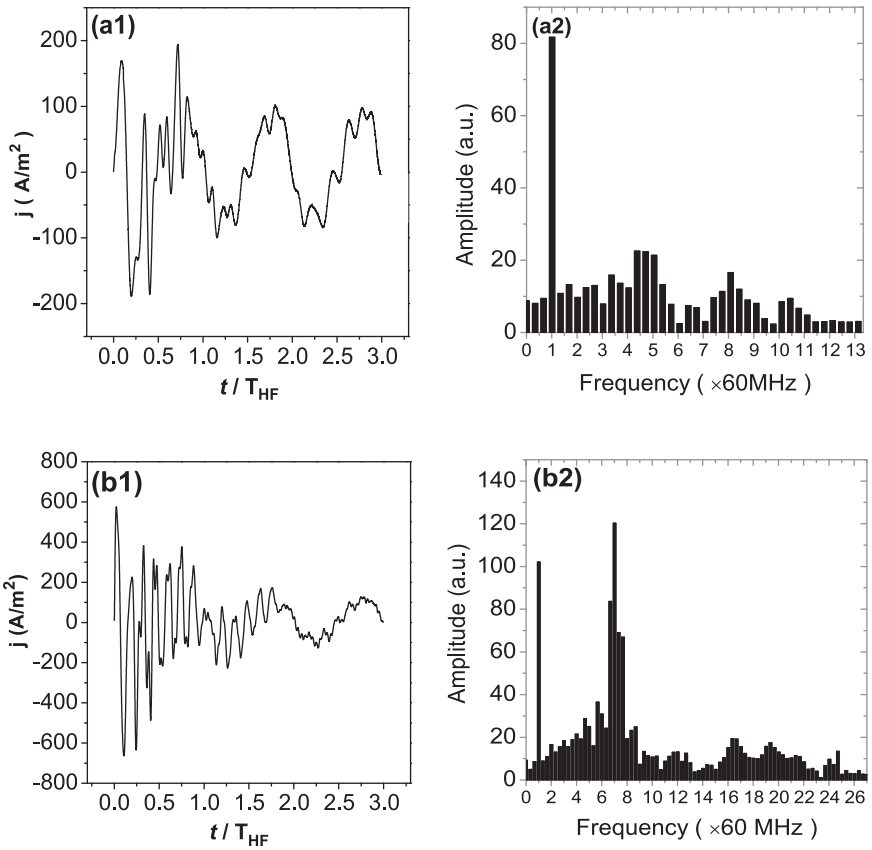

FIG. 9. (a1), (b1) Three full cycles of the HF current at the centre between the two electrodes, with $\theta = 90^\circ$. (a2), (b2): Fourier components of the current correspond to (a1) and (b1), respectively. (a1) represents the first three HF periods with the rise time defined in Sec. II above, whereas (b1) shows the results in the case of an instantaneous rise (i.e., rise time $\tau = 0$.)

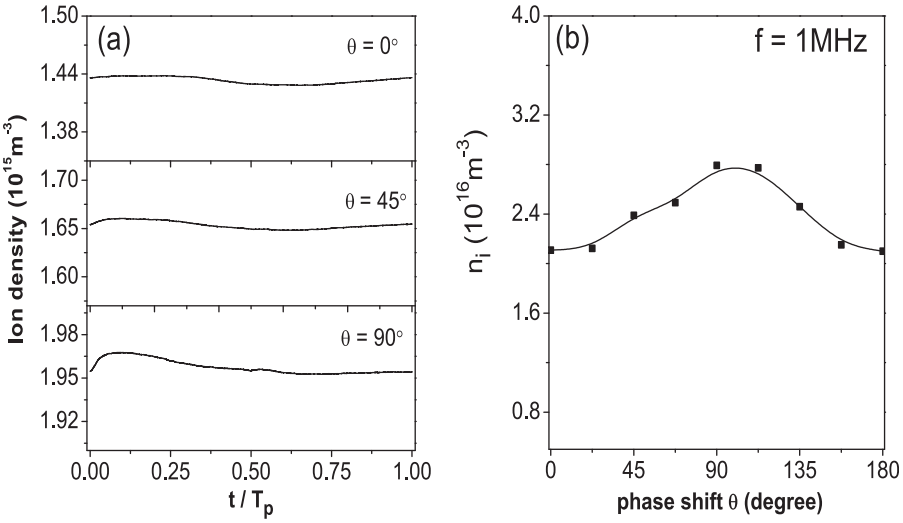

FIG. 10. (a) Spatially averaged Ar^+ densities as a function of time within one pulse modulation period for different phase shifts between the LF source and the pulse modulation, using a pulse modulation frequency of 1 MHz, and 0.5 duty cycle. (b) Spatially and time-averaged ion density versus the phase shift between the LF source and the pulse modulation for a pulse modulation frequency of 1 MHz.

the sudden change of HF voltage value in rise/fall time always exists.

C. Low frequency modulation

In this section, we examine the case of modulating the LF source with a pulse repetition frequency $f = 1$ MHz. Since the HF source voltage is now always present, also during the pulse-off time, the ion density changes slightly as a function of time (shown in Figure 10(a)). The time-averaged ion density shows the same trend as in the HF modulation for different phase shifts θ (shown in Figure 10(b)). Therefore, we mainly discuss the influence of pulse modulation on the IEDFs at the driven electrode, as presented in Figure 11(a).

Since the IEDFs are mainly determined by sheath potential, the latter is plotted as a function of time during one pulse modulation period in Figure 11(b). The first peaks (indicated with "1") shown in Figure 11(a) are caused by the HF (60 MHz) sources, which induces an identical potential drop ($-|V_{min}|$ in Figure 11(b)), and hence this explains why the energy of the first peak coincides for the three values of θ. The high-energy peaks (indicated with "2" in Figure 11(a)) are determined by different values of $-|V_{max}|$ (indicated with the subscript "1," "2," "3" in Figure 11(b)). With increasing θ from 0° to 90°, the maximum potential drop across the sheath, gradually decreases, $|V_{max}|_1 > |V_{max}|_2 > |V_{max}|_3$, as appears from Figure 11(b). This explains why the ion energy of the peak in Figure 11(a) (indicated with "2") also decreases. Note that the sheath potential is defined by the difference between the driven electrode potential and the maximum potential in the plasma as in Figure 4(b).

Moreover, Figure 11(b) illustrates that there is an abnormal change in the sheath potential due to the LF modulation at the start of the pulse-off time (i.e., $t = 0.5T_p$) when $\theta \neq 0°$, and the amplitude of this abnormal change becomes larger and sustains for a longer time with increasing θ. This leads to the third energy peaks in Figure 11(a) in the case of $\theta = 0°$ or 90°. Therefore, we can conclude that, in contrast to the modulation of the HF source, the IEDFs are affected by pulsing the LF source.

IV. CONCLUSIONS

Using a 1d3v PIC/MCC model including a bias capacitor, we investigate the behavior of the ion (or plasma) density, the IEDF, the ionization rate and the high frequency

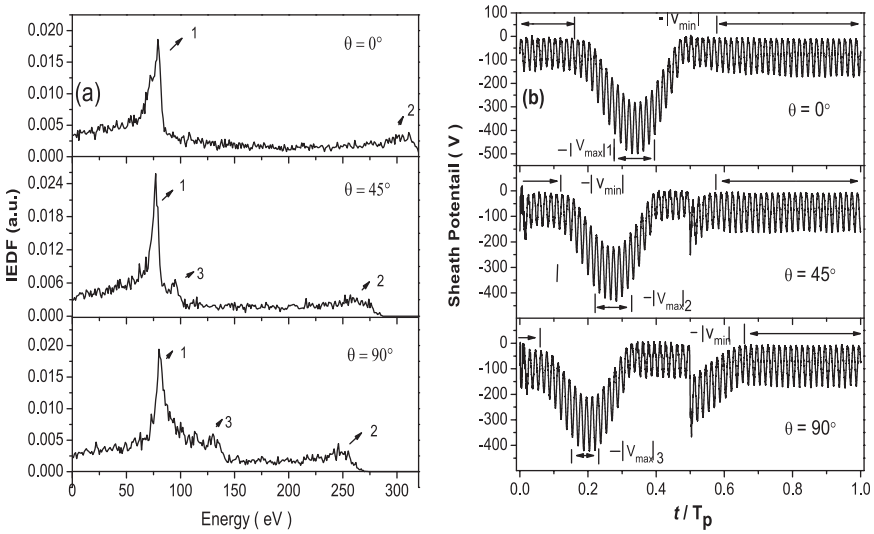

FIG. 11. (a) Time-averaged ion energy distribution functions (IEDFS) at the driven electrode, and (b) sheath potential as a function of time during one pulse modulation period, with LF modulation at f = 1 MHz, for $\theta = 0°$, 45°, 90°.

harmonics phenomena in a pulsed DF CCP. We found that time-averaged ion densities first increase and then decrease by adjusting the phase shift between the high frequency source and the pulse modulation from 0° to 180°, when the HF source is pulsed. When tuning θ, a sudden change of the voltage appears within the rise time of pulse-on time, which induces a strong asymmetry in the discharge, especially at $\theta = 90°$, so that many HF harmonics are excited. These HF harmonics lead to rapid sheath expansions and the latter give rise to a high ionization rate and ion density in the initial stage of the pulse-on time. In addition, we also found that a shorter rise time induces a stronger asymmetry and higher frequency harmonics. For comparison, the pulse modulation of the LF source is also studied, and it is found that the temporal evolution of the ion density changes slightly and also the IEDFs can be modulated to some extent, in contrast to the HF pulse modulation, where the IEDFs were found to be unaffected. This means that the HF pulse modulation opens up possibilities for independent control of ion energy and ion density (and flux). Moreover, the LF pulse modulation might be interesting to reduce the maximum ion bombarding energy, keeping a high ion density and flux.

ACKNOWLEDGMENTS

This work was supported by the National Natural Science Foundation of China (Grant Nos. 11335004 and 11275038), the Important National Science and Technology Specific Project (Grant No. 2011 ZX 02403–001), the International Science and Technology Cooperation Program of China (Grant No. 2012 DFG 02150), and the joint research project in the framework of the agreement between MOST and FWO-Flanders.

[1]M. A. Lieberman and A. J. Lichtenberg, *Principles of Plasma Discharges and Materials Processing*, 2nd ed. (Wiley, New York, 2005).
[2]G. S. May and S. M. Sze, *Fundamentals of Semiconductor Fabrication* (Wiley, New York, 2004).
[3]T. Kitajima, Y. Takeo, Z. L. Petrovic, and T. Makabe, Appl. Phys. Lett. **77**, 489 (2000).
[4]T. Denda, Y. Miyoshi, Y. Komukai, T. Goto, Z. L. Petrovic, and T. Makabe, J. Appl. Phys. **95**, 870 (2004).
[5]P. C. Boyle, A. R. Ellingboe, and M. M. Turner, J. Phys. D:Appl. Phys. **37**, 697 (2004).
[6]J. K. Lee, O. V. Manuilenko, N. Yu. Babaeva, H. C. Kim, and J. W. Shon, Plasma Sources Sci. Technol. **14**, 89 (2005).
[7]J. P. Booth, G. Curley, D. Maric, and P. Chabert, Plasma Sources Sci. Technol. **19**, 015005 (2010).
[8]V. Georgieva and A. Bogaerts, Plasma Sources Sci. Technol. **15**, 368 (2006).
[9]S. Wang, X. Xu, and Y. N. Wang, Phys. Plasmas **14**, 113501 (2007).
[10]M. M. Turner and P. Chabert, Phys. Rev. Lett. **96**, 205001 (2006).
[11]J. Schulze, T. Gans, D. O'Connell, U. Czarnetzki, A. R. Ellingboe, and M. M. Turner, J. Phys. D: Appl. Phys. **40**, 7008 (2007).
[12]M. Olevanov, O. Proshina, T. Rakhimova, and D. Voloshin, Phys. Rev. E **78**, 026404 (2008).
[13]Y. Yang and M. J. Kushner, J. Appl. Phys. **108**, 113306 (2010).
[14]S. K. Ahn and H. Y. Chang, Appl. Phys. Lett. **95**, 111502 (2009).
[15]Z. Donkó, J. Schulze, P. Hartmann, I. Korolov, U. Czarnetzki, and E. Schüngel, Appl. Phys. Lett. **97**, 081501 (2010).
[16]J. Waskoenig and T. Gans, Appl. Phys. Lett. **96**, 181501 (2010).
[17]B. G. Heil, U. Czarnetzki, R. P. Brinkmann, and T. Mussenbrock, J. Phys. D: Appl. Phys. **41**, 165202 (2008).
[18]Z. Donkó, J. Schulze, B. G. Heil, and U. Czarnetzki, J. Phys. D: Appl. Phys. **42**, 025205 (2009).
[19]J. Schulze, E. Schüngel, Z. Donko, and U. Czarnetzki, J. Phys. D: Appl. Phys. **43**, 225201 (2010).
[20]U. Czarnetzki, J. Schulze, E. Schüngel, and Z. Donkó, Plasma Sources Sci. Technol. **20**, 024010 (2011).
[21]Q. Z. Zhang, W. Jiang, L. J. Hou, and Y. N. Wang, J. Appl. Phys. **109**, 013308 (2011).
[22]T. Ohmori and T. Makabe, Appl. Surf. Sci. **254**, 3696 (2008).
[23]S. Ashida, C. Lee, and M. A. Lieberman, J. Vac. Sci. Technol. A. **13**, 2498 (1995).
[24]A. Agarwal, S. Rauf, and K. Collins, Appl. Phys. Lett. **99**, 021501 (2011).
[25]A. Agarwal, S. Rauf, and K. Collins, Appl. Phys. **112**, 033303 (2012).
[26]H. C. Kim, J. K. Lee, and J. W. Shon, Appl. Phys. Lett. **84**, 864 (2004).
[27]T. Lafleur, R. W. Boswell, and J. P. Booth, Appl. Phys. Lett. **100**, 194101 (2012).
[28]T. Lafleur and J. P. Booth, J. Phys. D: Appl. Phys. **45**, 395203 (2012).
[29]P. Diomede, D. J. Economou, and V. M. Donnelly, J. Appl. Phys. **109**, 083302 (2011).
[30]H. B. Smith, C. Charles, R. W. Boswell, and H. Kuwahara, J. Appl. Phys. **82**, 561 (1997).
[31]A. Mishra, M. H. Jeon, K. N. Kim, and G. Y. Yeom, Plasma Sources Sci. Technol. **21**, 055006 (2012).
[32]V. Samara, M. D. Bowden, and N. St. J. Braithwaite, J. Phys. D: Appl. Phys. **43**, 124017 (2010).
[33]J. P. Verboncoeur, M. V. Alves, V. Vahedi, and C. K. Birdsall, J. Comput. Phys. **104**, 321–328 (1993).
[34]V. Vahedi and G. DiPeso, J. Comput. Phys. **131**, 149 (1997).
[35]W. Jiang, H. Y. Wang, S. X. Zhao, and Y. N. Wang, J. Phys. D: Appl. Phys. **42**, 102005 (2009).
[36]H. Y. Wang, W. Jiang, and Y. N. Wang, Plasma Sources Sci. Technol. **19**, 045023 (2010).
[37]Q. Z. Zhang, S. X. Zhao, W. Jiang, and Y. N. Wang, J. Phys. D: Appl. Phys. **45**, 305203 (2012).
[38]Q. Z. Zhang, Y. X. Liu, W. Jiang, A. Bogaerts, and Y. N. Wang, Plasma Sources Sci. Technol. **22**, 025014 (2013).
[39]V. Georgieva, A. Bogaerts, and R. Gijbels, J. Appl. Phys. **93**, 2369 (2003).
[40]V. Georgieva and A. Bogaerts, J. Appl. Phys. **98**, 023308 (2005).
[41]L. Lauro-Taroni, M. M. Turner, and N. St. J. Braithwaite, J. Phys. D: Appl. Phys. **37**, 2216 (2004).
[42]M. Roberto, H. B. Smith, and J. P. Verboncoeur, IEEE Trans. Plasma Sci. **31**, 1292 (2003).
[43]A. V. Phelps and Z. L. Petrovic, Plasma Sources Sci. Technol. **8**, R21 (1999).
[44]V. Vahedi and M. Surendra, Comput. Phys. Commun. **87**, 179–198 (1995).
[45]M. M. Turner, Phys. Plasmas **13**, 033506 (2006).
[46]J. Liu, G. L. Huppert, and H. H. Sawin, J. Appl. Phys. **68**, 3916–3934 (1990).
[47]N. Yu. Babaeva, J. K. Lee, J. W. Shon, and E. A. Hudson, J. Vac. Sci. Technol. A **23**, 699–704 (2005).
[48]S. Banna, A. Agarwal, G. Cunge, M. Darnon, E. Pargon, and O. Joubert, J. Vac. Sci. Technol. A **30**, 040801 (2012).
[49]V. A. Godyak and R. B. Piejak, Phys. Rev. Lett. **65**, 996 (1990).
[50]W. Jiang, X. Xu, Z. L. Dai, and Y. N. Wang, Phys. Plasmas **15**, 033502 (2008).